CERN Summer Student Project Report 2020

Shower shapes and magnetic field in the ATLAS EM calorimeter

Student:
Erdenebulgan Lkhagvadorj
erdenebulganl@mas.ac.mn
Institute of Physics and Technology
Mongolian Academy of Science

Supervisor:
Julien Maurer
jmaurer@cern.ch
IFIN-HH, ATLAS experiment

August 27, 2020

Contents

1 Introduction

The context of this project is the CERN summer student remote program for the year 2020. During that remote activity, I had to learn Python and Root, therefore I started to learn how to use it to draw histograms and plots. Moreover, I presented my results in the Atlas EGamma meeting two times.

In the first data recorded by ATLAS in 2010, it was observed [1] that several of the shower shape variables were mis-modelled by the Monte Carlo (MC) simulation. In particular, comparing the R_η and $W_{\eta 2}$ distributions for signal electrons from $Z \rightarrow ee$ events, significant discrepancies between data and MC simulation can be seen in Figure (1). In order to explain these discrepancies, we want to consider the influence of the residual magnetic field in the calorimeter. We also looked for how big of the magnetic effect can involve. To quantify this, we did a simple comparison between two single-photon samples that have magnetic field either enabled or disabled. In addition, we had tested some samples with an influence of cross-talk, Birks' law, and Geant4 simulation.

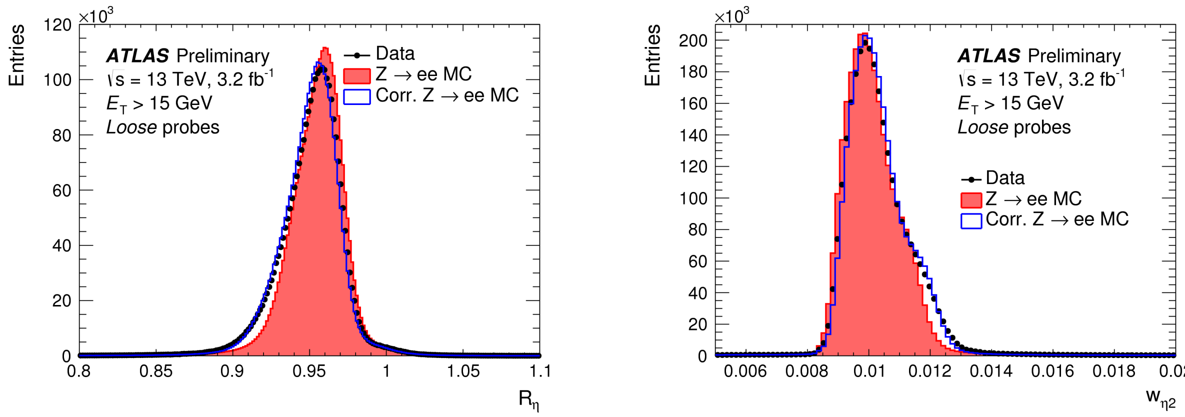

(a) Reta distribution

(b) Weta2 distribution

Figure 1: Data/MC comparisons of shower shapes.

2 ATLAS detector

The ATLAS detector [2] is a multi-purpose apparatus with a forward-backward symmetric cylindrical geometry and nearly 4π solid angle coverage. The inner detector consists of pixel and microstrip trackers covering $|\eta| < 2.5$ and a Transition Radiation Tracker (TRT) covering $|\eta| < 2.0$. The inner detector is located inside a thin superconducting solenoid. Outside the solenoid, a lead/liquid argon (LAr) electromagnetic (EM) calorimeter measures the energy and position of electrons and photons in the region $|\eta| < 3.2$. An iron/scintillating-tile calorimeter covers the region $|\eta| < 1.7$. A muon spectrometer surrounds the calorimeter system.

2.1 Electron reconstruction in ATLAS

Electron reconstruction [3], [4] in the precision region of the ATLAS detector ($|\eta| < 2.5$) proceeds along the following steps:

- localised clusters of energy deposits found within the EM calorimeter
- charged-particle tracks identified in the inner detector
- close matching $\eta \times \phi$ space of the tracks to the clusters to form the final electron candidates

- rejection of hadrons based on the shower lateral and longitudinal profiles and compatibility between track and cluster.

A schematic illustration of the elements that enter into the reconstruction and identification of an electron as shown in Figure (2).

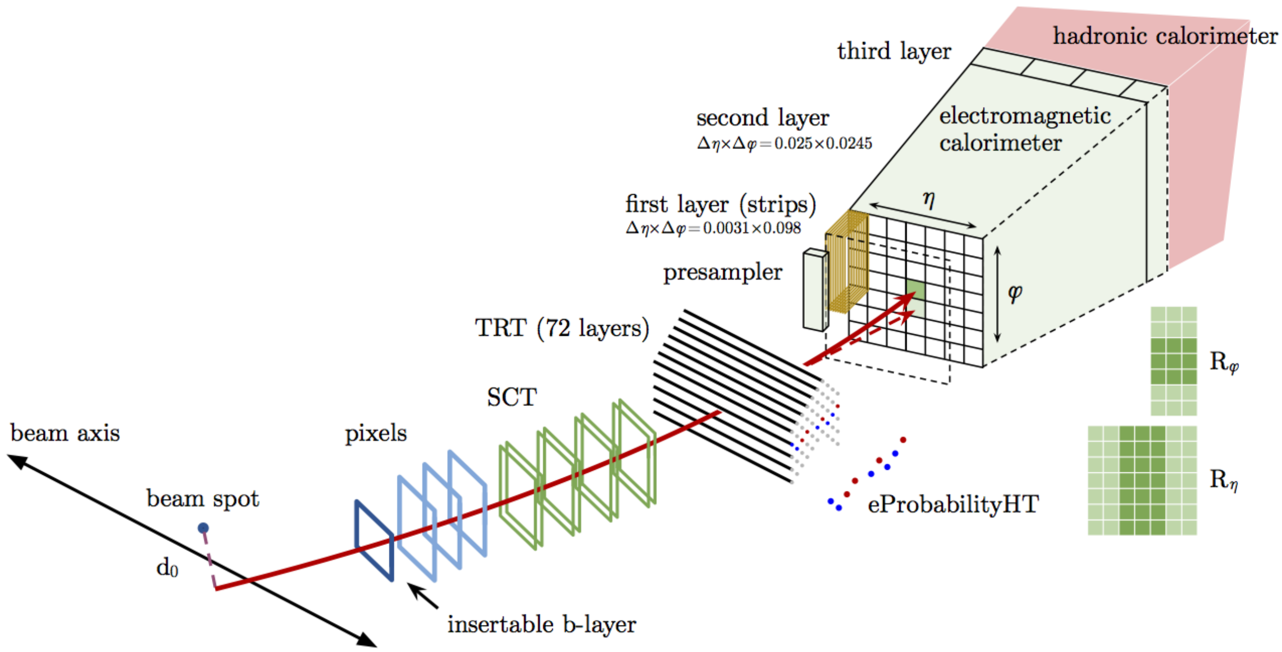

Figure 2: The illustration of the path of an electron through the detector [3]. The red trajectory shows the hypothetical path of an electron, which first traverses the tracking system (pixel detectors, then silicon-strip detectors and lastly the TRT) and then enters the electromagnetic calorimeter. The dashed red trajectory indicates the path of a photon produced by the interaction of the electron with the material in the tracking system.

2.2 Magnetic field in the calorimeter

Magnetic field can impact the development of the electromagnetic shower, by making secondary electron in the shower spiral along the liquid argon gaps. In Figure (3), the magnetic field in the barrel of the electromagnetic calorimeter (i.e. in the region $0 < |\eta| < 1.45$) is shown. The green rectangle represents the active area of the electromagnetic calorimeter. The orange rectangle also represents the coil of the solenoid magnet. The x-axis of the plot (labelled "Z") corresponds to the beam axis, while the y-axis (labelled "Y") corresponds to the vertical direction. The red numbers (e.g. 0.1T) indicate the magnitude of the magnetic field (in Tesla), which is also proportional to the spacing between the field lines.

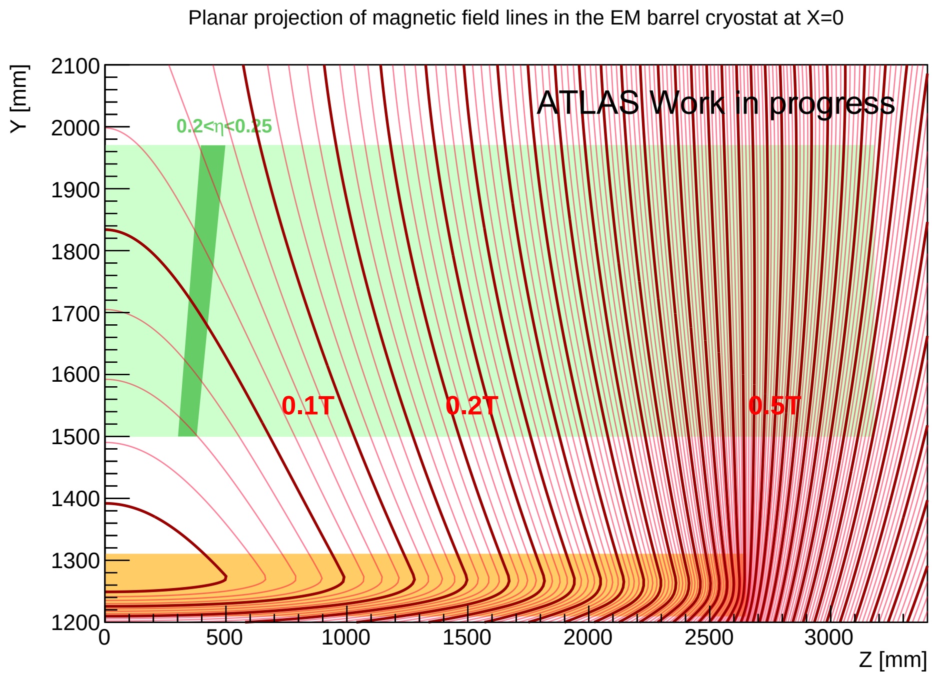

Figure 3: Magnetic field in the calorimeter

3 Results and discussion

Our main objective was to make plots comparing the distributions of a few interesting variables (such as transverse momentum, pseudorapidity, shower lateral profile) in order to see if the magnetic field has an effect on them.

- Transverse momentum (pT) – the component of momentum in the transverse plane.
- Pseudorapidity (η) – spatial coordinate describing the angle of a particle relative to the beam axis. It is defined as

$$\eta \equiv -ln\left[tan\left(\frac{\theta}{2}\right)\right],$$

  where θ is the angle between the particle three-momentum $\mathbf{p}$ and the positive direction of the beam axis.
- Shower lateral width (weta1) along the η direction in the first layer of the EM calorimeter – It corresponds more or less to the RMS of the energy deposits in 7 cells (the one with highest energy and 3 neighbours on each side):

$$W_{\eta 1} = \sqrt{\frac{\sum E_i (i - i_{max})^2}{\sum E_i}}.$$

  The unit of this variable is the number of layer-1 cells and typical values will be $O(0.5)$.
- Shower lateral width (weta2) along the η direction in the second layer of the EM calorimeter – It corresponds essentially to the RMS of the energy deposits in a set of 3 x 5 = 15 cells around

the estimated impact point of the photon in this layer:

$$W_{\eta 2} = \sqrt{\frac{\sum (E_i \eta_i)^2}{\sum E_i} - \left(\frac{\sum (E_i \eta_i)}{\sum E_i}\right)^2}.$$

The unit of this variable is the pseudorapidity, so typical values are $O(0.01)$, half the size of a cell in layer 2.

- Ratio of the energy in the η direction (Reta) – ratio of energy deposited in windows of 3 x 7 and 7x7 cells in the layer 2. Typical value is around 1.
- Ratio of the energy in the ϕ direction (Rphi) – ratio of energy deposited in windows of 3 x 3 and 3x7 cells in the layer 2. Typical value is around 1.

3.1 The samples with magnetic field either ON or OFF

Our single-photon particle gun samples have some properties which are listed below.

- Containing photons with $0.2 < |\eta| < 0.25$, and $pT = 65$ GeV.
- Photons are produced at a radius $R = 1148$ mm (after the inner detector).
- Shower shape distributions from xAODs.

$W_{\eta 1}$, $W_{\eta 2}$, R_η, and R_ϕ distributions are illustrated in the following figures (Figure 4(a) - 4(d)). In these plots, red shapes represent the sample with magnetic field otherwise black shapes represent the sample without magnetic field. We also performed a statistical test by χ_2 - test. All the distributions are consistent within statistical uncertainties through the statistical test.

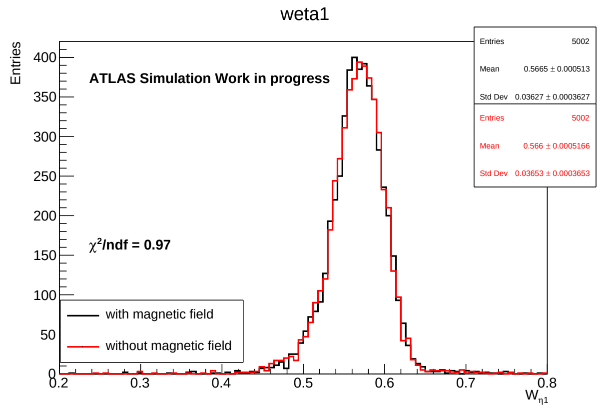

(a) Shower lateral width distribution in the first layer of the calorimeter

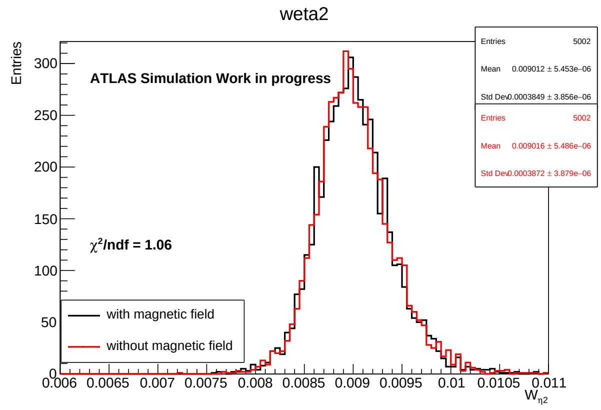

(b) Shower lateral width distribution in the second layer of the calorimeter

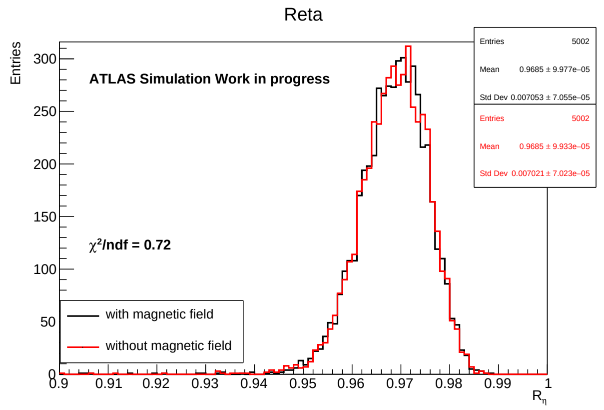

(c) Ratio of the energy distribution in the η direction

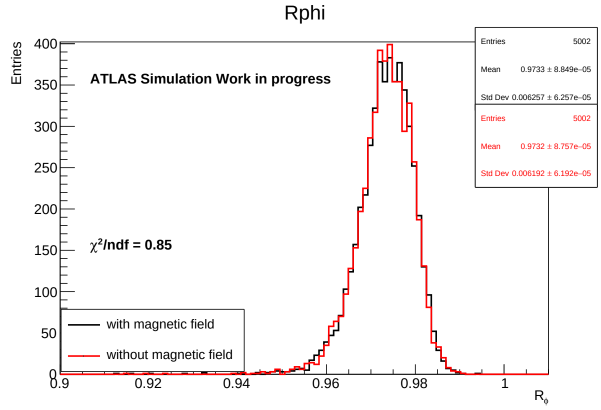

(d) Ratio of the energy distribution in the ϕ direction

Figure 4: Shower shapes of samples with magnetic field either ON or OFF.

Next test corresponds to a different pseudorapidity region ($\eta = 1.2$), which has also magnetic field either on or off, shown in Figure (5). According to the comparison between Figure (4) and Figure (5), the different pseudorapidity region didn't illustrate any changes for shower shapes except R_ϕ variable.

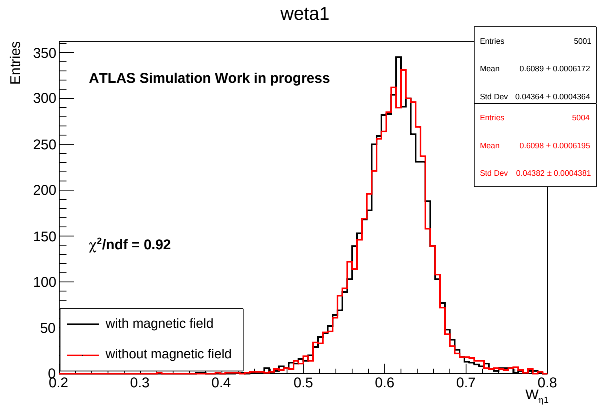

(a) Shower lateral width distribution in the first layer of the calorimeter

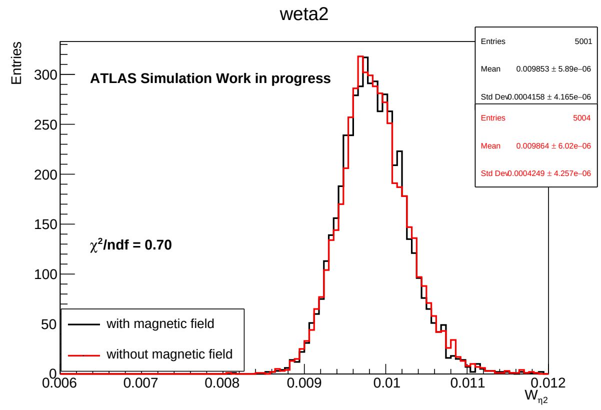

(b) Shower lateral width distribution in the second layer of the calorimeter

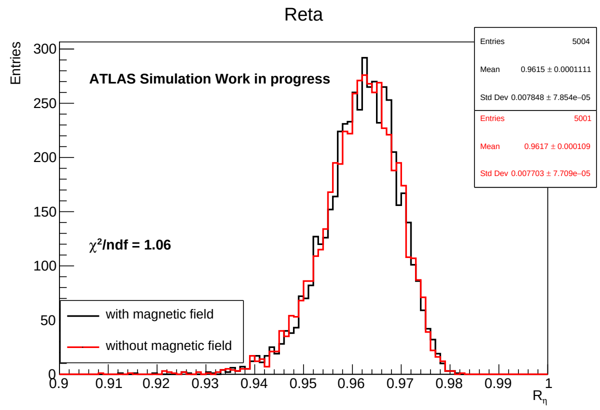

(c) Ratio of the energy distribution in the η direction

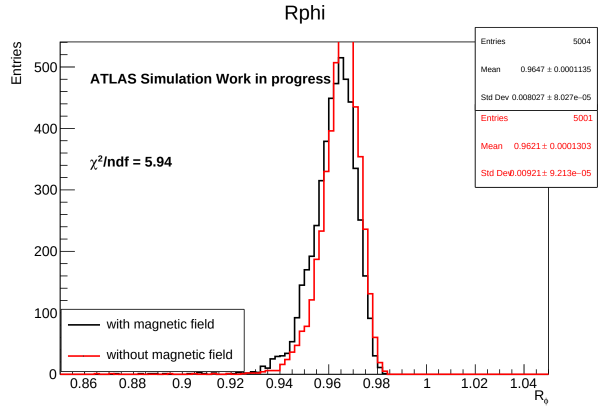

(d) Ratio of the energy distribution in the ϕ direction

Figure 5: Shower shapes of samples in $\eta = 1.2$ region.

3.2 The samples with cross-talk influences

A cell recording a physical or calibration signal originating from other cells is called cross-talk. There are two types of cross-talk: read-out cross-talk and charge collection cross-talk. The read-out cross-talk is capacitive, resistive and inductive couplings between the electrodes and read-out cables. In the charge collection cross-talk, ionization charges produced in the fiducial volume of one cell, drift into other cells due to the electric field and are collected there. In this samples, we consider three different samples:

- Magnetic field OFF, $\eta = 0.2$, read-out cross-talk in the first layer of the calorimeter DOUBLED
- Magnetic field OFF, $\eta = 0.2$, read-out cross-talk in the middle layer of the calorimeter DOUBLED
- Magnetic field OFF, $\eta = 0.2$, charge collection cross-talk OFF.

These three samples are compared against the sample with the magnetic field OFF, displayed in Figure (6).

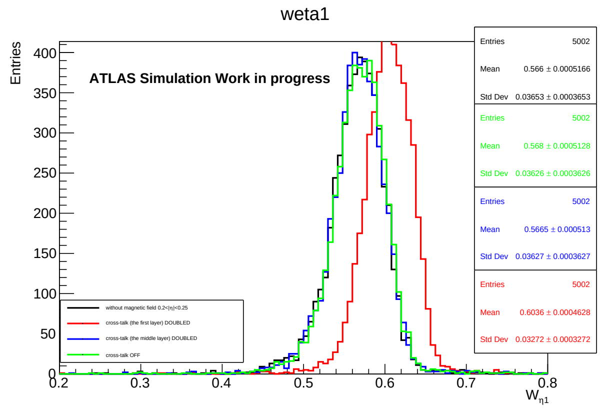

(a) Shower lateral width distribution in the first layer of the calorimeter

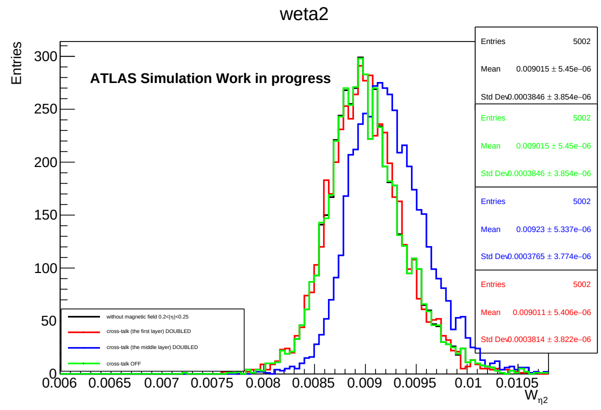

(b) Shower lateral width distribution in the second layer of the calorimeter

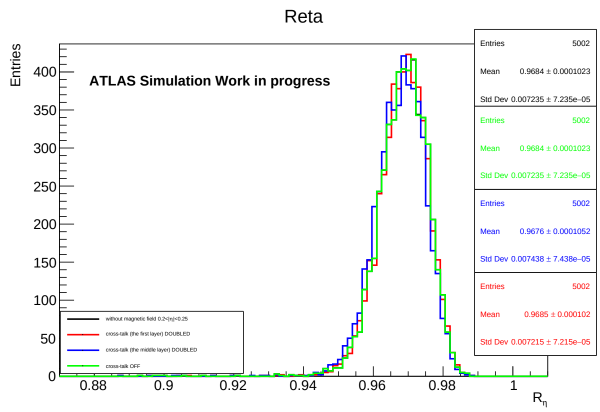

(c) Ratio of the energy distribution in the η direction

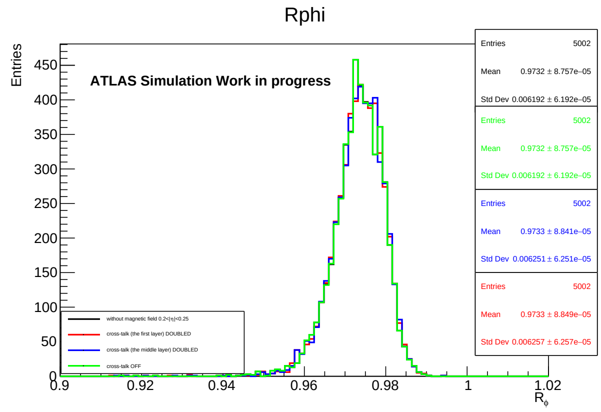

(d) Ratio of the energy distribution in the ϕ direction

Figure 6: Shower shapes of samples with cross-talk influences (magnetic field OFF).

3.3 The samples with Birks' law OFF

Birks' law is a formula for the light yield per path length as a function of the energy loss per path length for a particle traversing a scintillator.

$$\frac{dL}{dx} = S \frac{\frac{dE}{dx}}{1 + k_B \frac{dE}{dx}},$$

where L is the light yield, S is the scintillation efficiency, dE/dx is the energy loss of the particle per path length, and k_B is Birks' constant.

The sample, Birks' law disabled, is also compared against the sample without magnetic field. These plots are shown in Figure (7).

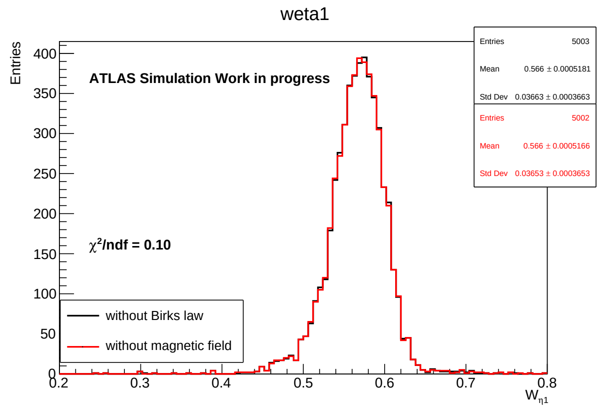

(a) Shower lateral width distribution in the first layer of the calorimeter

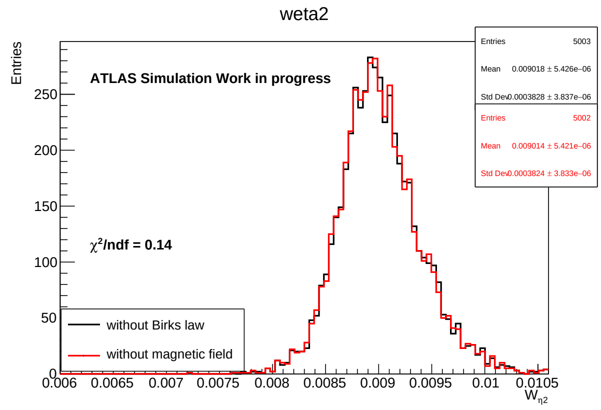

(b) Shower lateral width distribution in the second layer of the calorimeter

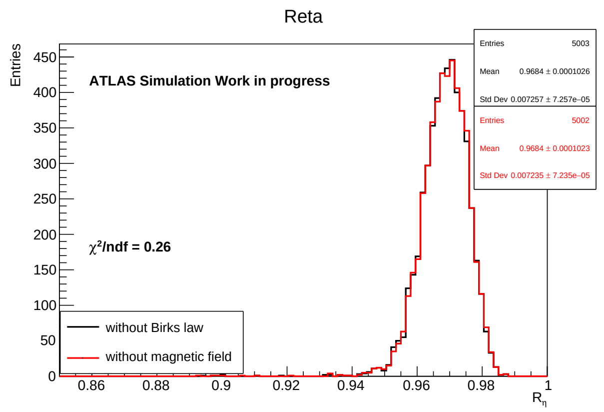

(c) Ratio of the energy distribution in the η direction

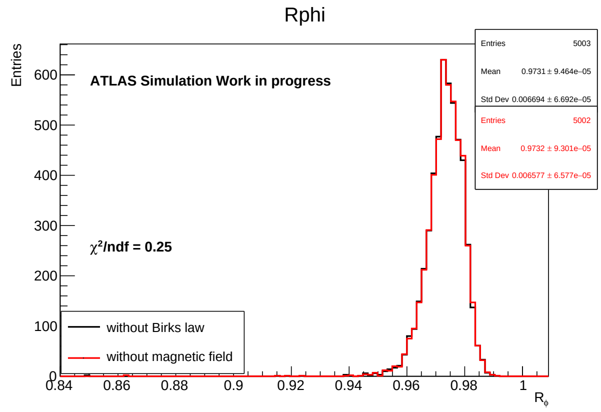

(d) Ratio of the energy distribution in the ϕ direction

Figure 7: Shower shapes of samples with Birks' law disabled (magnetic field OFF).

3.4 The samples using varied settings of Geant4 simulation

Finally, we tested two variations of the Geant4 simulation software:

- Magnetic field ON, $\eta = 0.2$, new Geant4 version (10.6),
- Magnetic field ON, $\eta = 0.2$, a higher precision physics list for the low-energy electromagnetic processes.

These two samples are also compared to ones with magnetic field, illustrated in Figure (8).

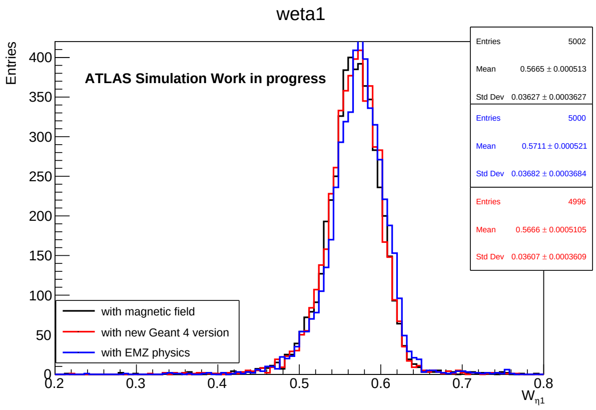

(a) Shower lateral width distribution in the first layer of the calorimeter

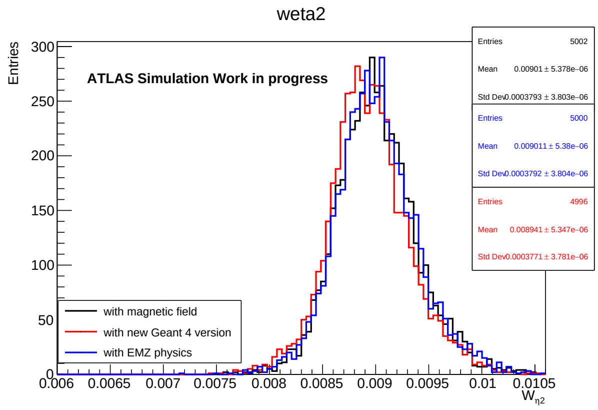

(b) Shower lateral width distribution in the second layer of the calorimeter

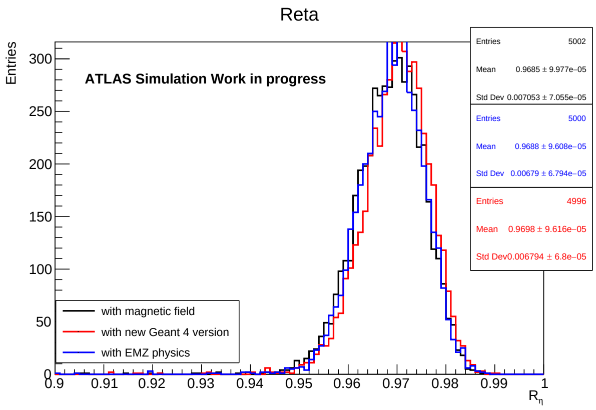

(c) Ratio of the energy distribution in the η direction

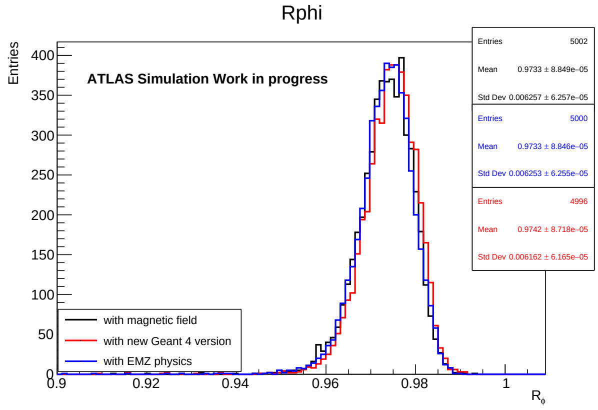

(d) Ratio of the energy distribution in the ϕ direction

Figure 8: Shower shapes of samples using Geant4 simulation (magnetic field ON).

4 Conclusion

During this remote project, we had tried to check some samples whether significant discrepancies between data and MC simulation in $Z \rightarrow ee$ event are explained.

- The differences between the shapes of the two distributions for $W_{\eta 1}$, $W_{\eta 2}$, R_{η}, and R_{ϕ} are not significant for the samples with magnetic field either enabled or disabled, but the magnetic field has an effect on R_{ϕ} for $\eta = 1.2$.
- According to the Birks' law samples, there is no impact for the all variables.
- In the samples with new Geant4 version 10.6, showers look slightly narrower in the middle.
- In the samples with a higher physics list for the low-energy electromagnetic processes, there are slightly broader showers in the first layer for $W_{\eta 1}$, but not really different in middle layer.
- For the influences of different cross-talk, it gives important impact on $W_{\eta 1}$ and $W_{\eta 2}$, but less impact on R_{η} and R_{ϕ}.

- So the effects from cross-talk or improved/higher-accuracy Geant4 simulation might play a role and should be investigated in more detail.

5 Acknowledgement

I would like to thank Dr. Julien Maurer for having supervised me during the remote CERN summer student program. Particularly for this interesting project which experienced with detector structure and computing. I also want to thank Michael Duehrssen who produced these samples for us.

References

[1] ATLAS Collaboration, "Electron efficiency measurements with the ATLAS detector using the 2015 LHC proton-proton collision data," ATLAS-CONF-2016-024.

[2] ATLAS Collaboration, "The ATLAS Experiment at the CERN Large Hadron Collider," JINST 3 (2008) S08003. doi:10.1088/1748-0221/3/08/S08003

[3] ATLAS Collaboration, "Electron reconstruction and identification in the ATLAS experiment using the 2015 and 2016 LHC proton–proton collision data at $\sqrt{s} = 13$ TeV," Eur. Phys. J. C 79 (2019) 639. doi:10.1140/epjc/s10052-019-7140-6

[4] ATLAS Collaboration, "Electron and photon performance measurements with the ATLAS detector using the 2015–2017 LHC proton–proton collision data," JINST 14 (2019) P12006. doi: 10.1088/1748-0221/14/12/P12006